LAWRENCE
LIVERMORE
NATIONAL
LABORATORY

LLNL-JRNL-544136

Evaporite Caprock Integrity: An experimental study of reactive mineralogy and pore-scale heterogeneity during brine-CO2 exposure.

M. M. Smith, Y. Sholokhova, Y. Hao, S. A. Carroll

April 2, 2012

Environmental Science & Technology

Disclaimer

This document was prepared as an account of work sponsored by an agency of the United States government. Neither the United States government nor Lawrence Livermore National Security, LLC, nor any of their employees makes any warranty, expressed or implied, or assumes any legal liability or responsibility for the accuracy, completeness, or usefulness of any information, apparatus, product, or process disclosed, or represents that its use would not infringe privately owned rights. Reference herein to any specific commercial product, process, or service by trade name, trademark, manufacturer, or otherwise does not necessarily constitute or imply its endorsement, recommendation, or favoring by the United States government or Lawrence Livermore National Security, LLC. The views and opinions of authors expressed herein do not necessarily state or reflect those of the United States government or Lawrence Livermore National Security, LLC, and shall not be used for advertising or product endorsement purposes.

Evaporite Caprock Integrity: An experimental study of reactive mineralogy and pore-scale heterogeneity during brine-CO_2 exposure

AUTHORS *Megan M. Smith*, Yelena Sholokhova, Yue Hao, and Susan A. Carroll*

AUTHOR ADDRESS Lawrence Livermore National Laboratory, 7000 East Avenue L-231, Livermore, CA 94550, United States.

KEYWORDS geologic carbon sequestration; caprock stability; evaporite; anhydrite; dolomite; fracture; x-ray tomography; enhanced oil recovery

ABSTRACT

We present characterization and geochemical data from a core-flooding experiment on a sample from the Three Fingers evaporite unit forming the lower extent of caprock at the Weyburn-Midale reservoir, Canada. This low-permeability sample was characterized in detail using X-ray computed micro-tomography before and after exposure to CO_2-acidified brine,

allowing mineral phase, surface area, and voidspace distributions to be quantified in three dimensions. Solution chemistry indicated that CO_2-acidified brine preferentially dissolved dolomite until saturation was attained, while anhydrite remained unreactive. Steady dolomite dissolution contributed to increases in bulk permeability through the formation of a localized channel, guided by microfractures as well as porosity and reactive phase distributions aligned with depositional bedding. An indirect effect of carbonate mineral reactivity is voidspace generation through physical transport of anhydrite and silicates freed from the rock matrix following dissolution of dolomite. Reservoir management practices for both geologic carbon sequestration and CO_2-enhanced oil recovery should consider the effect of carbonate reactivity and the likelihood of creating fractures on caprock stability. The development of high permeability fast pathways in our experiment points to the need for characterization of carbonate content and fracture orientations in potential evaporite caprock formations.

INTRODUCTION

Several large-scale carbon capture and sequestration projects have been implemented as one response to rising atmospheric levels of carbon dioxide.[1] Deep saline aquifers, unmineable coal seams, thick basaltic sequences, and depleted oil and gas fields have all been considered as possible storage reservoirs.[2] Essential to long-term carbon storage efficiency of any reservoir class, however, is the integrity of an impermeable caprock layer, which provides protection against upward leakage of buoyant free-phase CO_2 or CO_2-saturated reservoir fluids into overlying strata and back to the atmosphere. Understanding the impact of mechanical and chemical stresses (e.g., fluctuating reservoir pressure conditions, changing fluid-rock equilibria, etc.) resulting from CO_2 injection on caprock integrity is an active area of research.[3-9]

Thick anhydrite sequences may provide an effective seal for carbonate hydrocarbon reservoirs, because evaporite layers have both a very low intrinsic permeability and a much higher CO_2 breakthrough pressure compared to other low-permeability siliciclastic formations.[11] Sealing effectiveness of evaporite formations for geologic carbon storage (GCS) may be further enhanced because sulfate minerals do not dissolve in direct response to CO_2-generated acidity. Sulfate mineral stability to CO_2-rich fluids stands in strong contrast to the increased solubility of carbonate minerals also prevalent in evaporite sequences. However, preferential dissolution of carbonate phases within a multi-mineralic caprock sequence has the potential to compromise an otherwise impermeable overburden.[8,11]

In this paper we focus on the roles of reactive versus stable mineralogy and pore-scale heterogeneity in the development of preferential flowpaths within an evaporite sample which serves as a model for anhydrite caprocks overlying carbonate reservoirs. The experiment used core from the Three Fingers formation, the lower extent of caprock at the IEA GHG Weyburn-Midale Monitoring and Storage Project, Saskatchewan, Canada,[12] and was conducted under near *in situ* pressure, temperature, and brine conditions observed at the site.[13,14] Changes in permeability, solution chemistry, and mineral and void distributions were used to assess the evolving relationships among porosity and mineral reactivity throughout the impermeable core.

EXPERIMENTAL

We conducted a core-flooding experiment on a 30mm-long, 15mm-diameter subcore, drilled parallel to bedding, from the Three Fingers evaporite formation within the Midale Marly sequence. The core was taken from wellbore 21/6-8-6-13W2, drilled prior to CO_2-enhanced oil

recovery (CO_2-EOR) operations at the Weyburn-Midale field. The characterization and experimental procedures are similar to those described in detail in a previous study.[15]

Sample Characterization

The Three Fingers formation consists of alternating layers of anhydrite and dolomite as [$Ca_{1.08}Mg_{0.92}(CO_3)_2$], and is accompanied by up to 30% silicates, primarily quartz and potassium feldspar.[16] We performed calibrated analysis of X-ray computed microtomography (XCMT) data to characterize the 3D voidspace and mineralogy content of the core both before and after brine/CO_2 exposure. XCMT analysis was conducted at ID-19 beamline, ESRF, Grenoble, France before reaction, and at the 8.3.2 beamline, ALS, Berkeley, California after reaction. Initial resolution at each of the synchrotron facilities was ~5 μm/pixel. To manage image size, XCMT data were rescaled to 14.8 μm/pixel using ImageJ software[17] with no loss of gray-scale resolution. Analysis of unreacted and reacted zones was conducted on a representative sampling of higher-resolution scanning electron microscopy (SEM) images to calibrate the XCMT gray-scale to specific voidspace, mineral distributions, and surface areas following the methods of Peters[18] (Figure 1, Table 1). Automated segmentation between dolomite and quartz was problematic due to their similar grayscale values. Visual differentiation between the two phases was possible through grain morphologies (euhedral dolomite rhombs vs. pitted, ragged quartz grains) and energy-dispersive spectroscopic (EDS) analysis. A representative core collected within 5 cm of the sample was also subjected to mercury intrusion porosimetry to estimate pore throat diameter distribution.

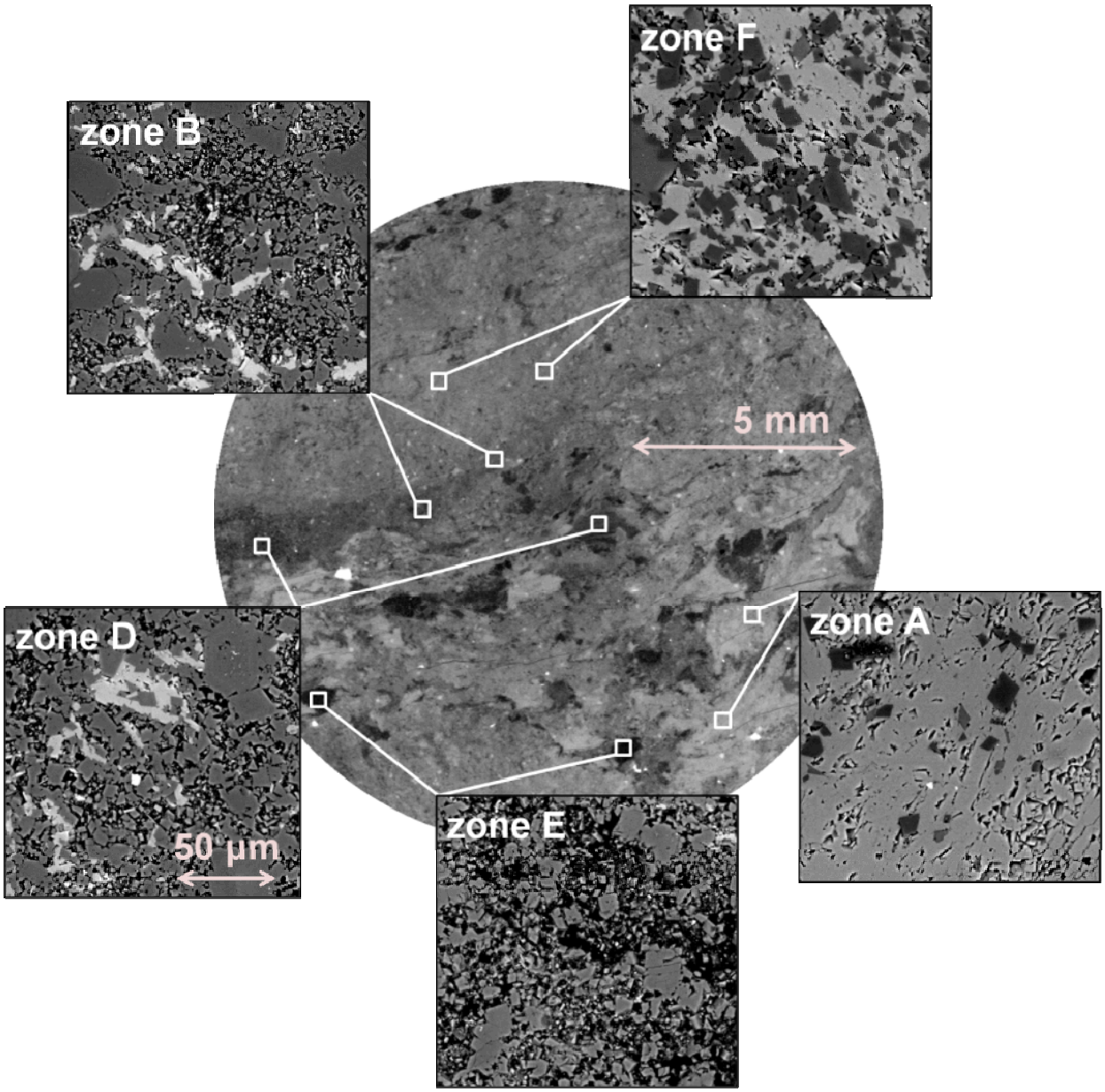

Figure 1. Representative tomography image, viewed perpendicular to core *z*-axis and located 3 mm from inlet face, showing identified gray-scale zones. Voidspace is shown as black, and lower-density solid phases (e.g., anhydrite, pyrite) are shown in the lightest shades. Note microfractures (visible above zone A inset) aligned along depositional layering at ~15° above horizontal.

Table 1. Composition of identified gray-scale XCMT zones. Propagated errors in porosity, anhydrite, and dolomite contents are ≤15%.

Interrogated Zones	porosity	anhydrite	dolomite	anhydrite ASSA*	dolomite ASSA
	%, total core volume			cm^{-1}	
Zone A, [131 255] moderate porosity, anh-rich	17.8	75.7	6.5	41,840	2,010
Zone B, [86 103] high porosity, dol-rich	27.0	12.4	60.6	6,290	26,790
Zone D, [74 85] high porosity, dol-rich	25.5	10.1	64.4	5,910	25,650
Zone E, [0 73] very high porosity, dol	51.6	0	48.4	0	19,940
Zone F, [104 130] low porosity, anh/dol	8.0	46.8	45.2	24,490	22,240

*"ASSA" refers to accessible specific surface area.

Core-Flooding Procedure

The core and two radially-bored endcaps were heat-shrink jacketed with Viton® to prevent bypass flow and vertically plumbed into the core-flooding apparatus[15] under constant 60°C and 24.8 MPa confining pressure conditions. Reactive flow was conducted under constant pressure conditions for ~11.5 days, until flowrates increased significantly as a result of "breakthrough" of a preferential pathway. The flowrate was then set at 0.05 mL/min for an additional 36 hours while two final fluid samples were collected. The brine composition (SI Table 1) was formulated to be near equilibrium with anhydrite and slightly supersaturated with

respect to both calcite and dolomite, in agreement with field observations. CO_2-free brine flow was monitored prior to reactive flow to establish baseline permeability and solution chemistry values, before introduction of reactive brine equilibrated with a pCO_2 of 3 MPa. System temperatures, pressures, and flowrates were collected continuously.

Filtered fluid samples were collected separately for element (by ICP-MS), ion (by IC), and total inorganic carbon (TIC) analysis. Effluent pH was measured prior to CO_2 introduction, and afterward was modeled via charge balance and solution chemistry data using code EQ3/6, Pitzer's equations, and *data.ypf* database.[19] Dolomite saturation (1.3 ± 0.3, relative to the *ypf* database) was previously defined in core-flooding experiments using permeable Marly dolostone cores which demonstrated sustained periods of steady-state carbonate dissolution behavior.[15] A simple linear interpolation with time was used to adjust elemental concentration data to TIC collection time to correct for the time lapse between these two samples during very slow flow during the first 10 days of reaction. Time corrections, chemical analysis errors, and variations in fluid flux rates were all incorporated into cumulative errors for dissolved load estimates.

RESULTS & DISCUSSION

Sample mineralogy and voidspace distributions

The composition of this Three Fingers subcore agreed well with extensive previous petrographic characterization.[16] The sample consisted primarily of layered regions of well- to poorly-cemented mixtures of anhydrite and dolomite, with much lesser quantities of pure dolomite and relatively pure anhydrite. Higher abundances of anhydrite were prevalent

immediately at the inlet and decreased in abundance with distance from the inlet (Figure 2). Porosity (averaged over core cross-section) was limited to intergranular space, increasing in less well-cemented (i.e., anhydrite-poor) regions, with the majority of pores dimensions less than 1-5 μm. Both dolomite and average porosity increased smoothly with distance from the inlet. Although the vast majority of pores were below the resolution of the tomography analysis, a mean pore throat diameter of 0.1 μm was determined by mercury intrusion porosimetry (SI Figure 1). Visible microfractures of ~5 μm diameter and up to 5 mm length occurred within anhydrite-rich regions and were aligned parallel to bedding. These small pore/aperture scales corroborated the measurement of a low initial permeability value (0.5 μDarcy) during CO_2-free brine flow periods. Silicate content in the sample was estimated at less than 10% of total core volume. Trace quantities of aluminosilicate clays as well as pyrite (small distinctly bright spots in Figure 1) were also confirmed via EDS spot analyses.

SEM photomicrographs of identified XCMT gray-scale zones provided more thorough characterization of the sample into five matrices, or zones (Figure 1, Table 1). Most visible microfractures occurred within zone A, which was identified as rare (1-8% of total sample volume) patches of relatively pure anhydrite, generally surrounded by the far more abundant zone F (40-65%; Figure 2e). These microfractures often extended laterally into and terminated within zone F, which was characterized by equal proportions of anhydrite and dolomite with the lowest observed porespace (8%). In contrast, zones B and D were the two most dolomite-rich regions, with consistently high accessible dolomite surface areas and porosities (26, 27%). These zones, while present at the inlet face and throughout the core, were never observed to host microfractures. The volumetric abundances of both B and D increased at the expense of the low-porosity zone F with increasing *z*-distance, contributing to the overall increase in dolomite

abundance seen in Figure 2c. The type locality for the fifth zone, zone E, was a distinctly banded ~4 mm carbonate fragment, extending from $9.5 < z < 14.5$ mm, which deformed the layers surrounding it (image not shown). This zone consisted of pure dolomite with high accessible surface area and very little anhydrite cement, and as a result it also was characterized by extremely high porosity (52%). Given both the chemical and physical likelihood for porous flow in this zone, it was important to capture its location with XCMT segmentation. However, it proved difficult to distinguish this region by gray-scale alone, and at other *z*-locations the segmentation procedure likely overestimated the abundance of zone E at the expense of other high-porosity regions (i.e., zones B and D).

Post-reaction XCMT imaging showed that CO_2-induced dissolution proceeded in localized regions, resulting in a preferentially dissolved channel (Figure 2a,b). This phenomenon of fast pathway or "wormhole" development has been documented extensively in the literature related to acidization of hydrocarbon reservoirs for enhanced oil recovery.[20-22] Several studies have correlated bulk flowrates with dissolution regimes, with slower flowrates favoring more strongly localized dissolution morphologies and increasing flowrates creating highly branching channels.[23,24] Given the variable flowrates observed in this experiment as a result of initially low permeability and spatially variable reactive phase distributions, we attempt instead to correlate CO_2-induced dissolution features with pre-existing mineralogy and voidspace distributions defined by the five zones discussed above and in Table 1.

Comparison of the initial composition of the dissolved region versus the make-up of the total core is shown in Figure 2c-f, demonstrating the combined influence of increased porosity and reactive phases (see SI Figure 2 for a visual breakdown of wormhole volume by zone). At the inlet face, 5-6 discrete wormholes initially formed in microfractures within zones A or F.

More porous and chemically reactive volumes of zone B were also abundant near the inlet (up to 25-30% of total sample volume; Figure 2e) but were not preferentially dissolved, demonstrating the strong influence of the much higher permeability fractures. As a result of discontinuity between microfractures, however, several initial wormholes died out early on, with only two persisting beyond z = 1.7 mm. At z = 4 mm, the fracture guiding the center wormhole ended, leaving a single ~0.7 mm diameter wormhole to transport fluid. The narrow channel diameter at this point resulted from dissolution of the available 10-20% dolomite (Figure 2d). As the last guiding fracture terminated into zone E (z = 9.5 mm), the single channel widened significantly, reaching up to 2 mm in diameter. After traversing the full extent of zone E, the wormhole then began to branch into several channels of variable diameter as it preferentially dissolved large volumes of zones B and D. The branching nature of the wormhole at this point implied that the porespace in these two zones was better connected, allowing for more fluid propagation and mineral dissolution in transverse directions. The branching dissolution pathways contrasted with the single-channel morphology noted in the fractured portions of the core, but the branches themselves remained confined in specific zones oriented parallel to the core's long axis (Figure 2a,b).

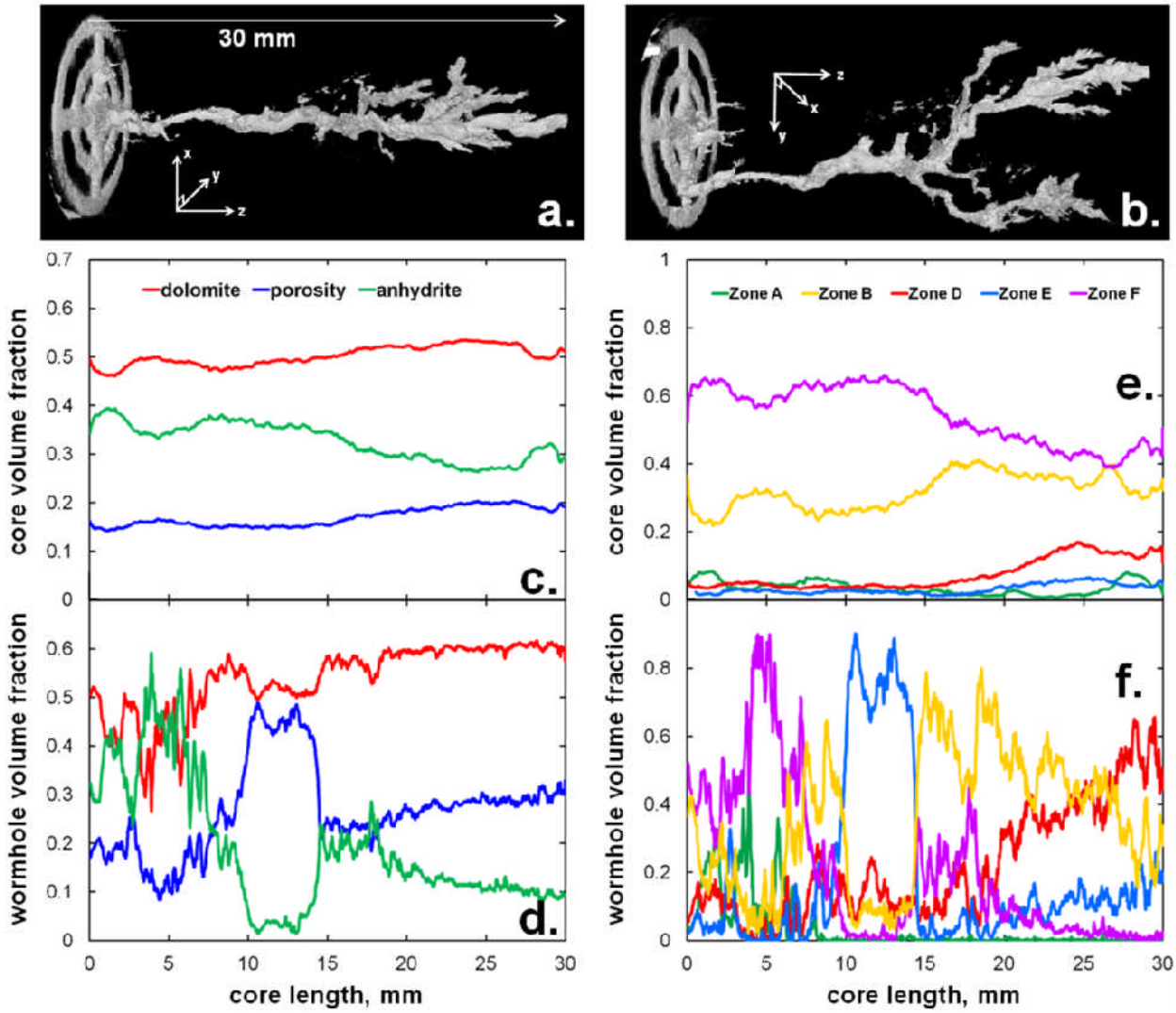

Figure 2. XCMT image of post-reaction wormhole formed by dissolution, from a) side view and b) after 90° rotation. The arrow denotes both the length of the core and the direction of flow. Also shown in is pre-reaction mineral and porosity content of c) the total core volume and d) the wormhole region only, as well as distribution of gray-scale zones throughout e) the total core volume and f) the wormhole region only, versus sample length.

Reactivity of Three Fingers Evaporite

CO_2-equilibrated brine flow was maintained through the 3-cm core at 0.004 ± 0.001 mL/min under a 9.65 MPa pressure gradient for over 6 days. Gradual flowrate increases were noted after 6 days, but significant flowrate (and permeability) increases did not occur until ~10 days, coincident with the attainment of steady-state TIC concentrations and drop in solution pH (Figure 3). We refer to this amount of time necessary to establish an interconnected, low-resistance fluid pathway through the core as the breakthrough time. During pre-breakthrough time, *bulk* permeability, calculated from pressure and flowrate data, increased by almost two orders of magnitude. After breakthrough and imposition of a constant fluid flowrate, differential pressures continued to decrease for 14 hours to below transducer resolution, indicating that the permeability within the established dissolution channel continued to increase.

Fluid saturation indices show that the CO_2-free brine ($t < 0$) was supersaturated with respect to carbonate minerals (including calcite, although it was not found in this sample) and at equilibrium or slightly undersaturated with anhydrite. Once CO_2-acidified brine was introduced to the sample, the system quickly readjusted within one day to dolomite saturation, with increasing amounts of dolomite continuing to dissolve until breakthrough (Figure 4). The short adjustment period for dolomite saturation is consistent with dolomite dissolution kinetics observed in previous core-flooding experiments using samples from underlying Weyburn-Midale formations.[15] Fluids maintained anhydrite saturation with minimal if any anhydrite dissolution. The lack of anhydrite dissolution was expected because anhydrite solubility does not depend on CO_2-induced pH decreases, and the input brine was designed to be in equilibrium with this mineral. Quartz remained undersaturated at all times, while secondary alteration minerals such as kaolinite and other aluminosilicate clays quickly became supersaturated. Silicate content was low

in this sample (~10-15%) and reaction kinetics for these phases are generally orders of magnitude slower than either dolomite or anhydrite. Chemical contribution of silicates to changes in porespace is likely to be negligible.

Solution pH decreased by almost two units to attain a steady value of ~5.2 in less than two days after the introduction of CO_2-acidified brine, similar to the timescale over which dolomite saturation indices evolved (Figures 3, 4). These effluent pH values still remained one unit higher than input pH (4.2 for 3 MPa pCO_2 brine), indicating ongoing carbonate buffering. TIC concentrations, however, required the full breakthrough time to achieve a steady-state level of 0.36 mol/L. The discrepancy between dolomite buffering and the slower increase of TIC could result from either experimental artifacts related to brine equilibration, or the influence of diffusion into an immobile porespace fraction (increasing with time) capable of delaying dissolved carbon transport. The input brine solution was allowed nearly two days to equilibrate with CO_2, a period long enough for equilibration according to recent measurements.[25] High concentration gradients between resident brine with low TIC concentrations and inflowing CO_2-equilibrated brine (8 vs. 360 mmol/L) could provide a strong driving force for diffusion into the evaporite matrix, especially in more porous regions such as zones B and D.

Once breakthrough of the fast pathway occurred (t > 10 days), the relative saturation of all phases except anhydrite dropped below zero as solution pH decreased further. Figure 5 shows an example image of the resulting highly porous reaction zone evident around portions of the wormhole by the end of the experiment (~0.64 porosity within the reacted region by t = 13 days). In this reacted region, the extent of dolomite dissolution decreased towards the unaltered evaporite matrix, over a lengthscale of 50-200 μm beyond the fully dissolved wormhole channel. This trend, together with the lack of evidence for anhydrite dissolution from solution chemistry

analyses, suggests that dolomite dissolution at grain boundaries left behind a residual anhydrite "skeleton." Once the evaporite matrix was sufficiently weakened by prolonged exposure to CO_2-acidified fluids, the residual anhydrite (or other chemically stable, e.g. quartz) solids were flushed out and were either retained on sample filters, or trapped in dead-end channels or within the walls of downstream matrix material.

Carbonate precipitation kinetics have been invoked as a potential method of "healing" fractures or slowing CO_2 transport through a compromised formation, given sufficiently high carbonate contents.[26] More specifically for evaporite systems, porosity reductions as a result of anhydrite precipitation,[27] or calcite precipitation driven by dedolomitization[28] or anhydrite reactivity[29] have been predicted to occur under high pCO_2 brine conditions. Examination of post-reaction images and solution chemistry from this work showed no evidence of precipitation of any mineral phases in or along the dissolved wormhole. Although the resolution of post-reaction XCMT data would preclude observation of precipitates smaller than ~10 μm (particles large enough to clog pore throats), solution chemistry and pressure data do not support sustained precipitation of any phase. In addition, the experimental brine composition was formulated to resemble a typical *in situ* brine, in or near equilibrium with primary reservoir minerals, and thus high sulfate concentrations kept anhydrite stable. Dolomite dissolution released additional dissolved calcium to the system, but at levels too low to force anhydrite or calcite precipitation under local pH conditions.

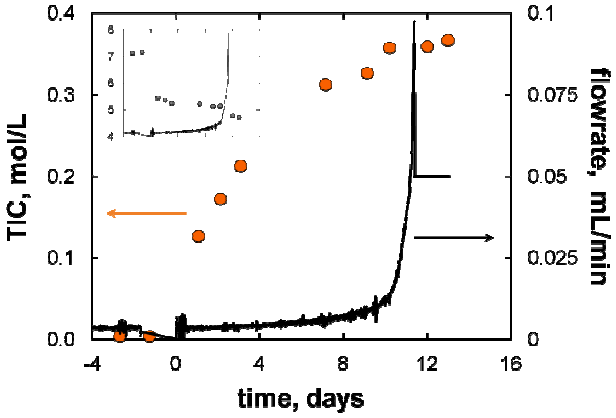

Figure 3. Total inorganic carbon (TIC) concentration (circles; left y-axis) and flowrate (black line; right y-axis) versus time. Solution pH versus time is also shown as an inset plot over the same timescale.

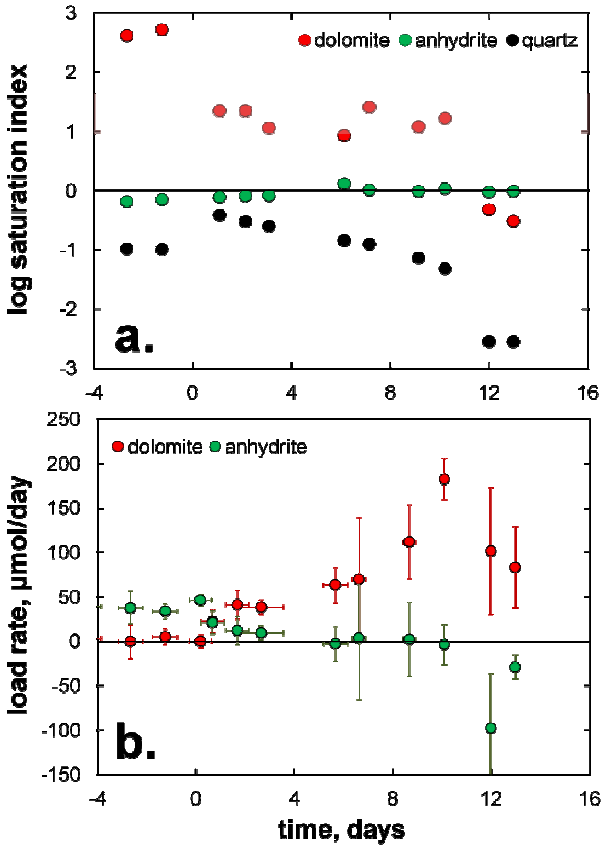

Figure 4. a) Log fluid saturation indices and b) instantaneous mineral load rates versus time. The shaded region in a) indicates previously experimentally determined extent of dolomite saturation.[15] Note that a positive load rate in b) indicates mineral dissolution.

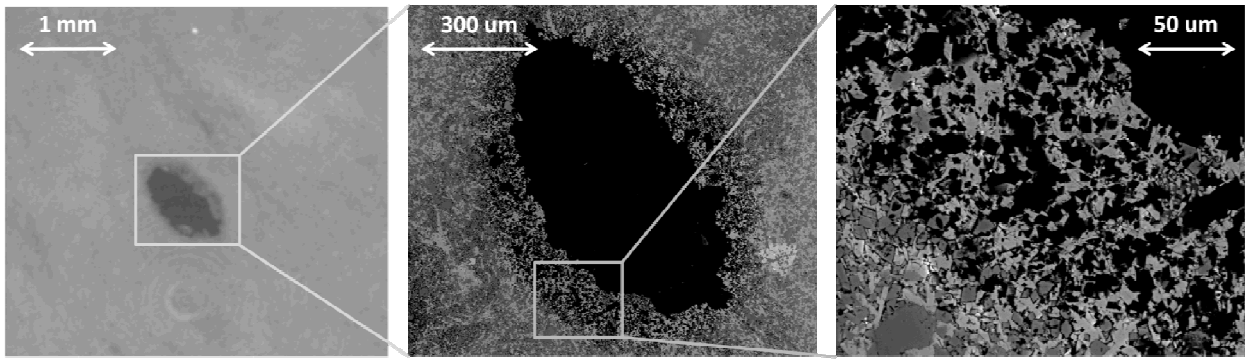

Figure 5. XCMT image and two SEM magnification of reacted edge of wormhole, taken 21 mm from inlet.

Implications for evaporite caprock stability

Reservoir management practices for both GCS and CO_2-EOR should consider the effect of carbonate reactivity and the likelihood of creating fractures on caprock stability. The development of high permeability fast pathways in a dolomitic evaporite in our experiment points to the need for characterization of both fracture orientations and carbonate content in potential evaporite caprock formations.

Local heterogeneity exerts a strong control on the location of preferential pathways at the micro-scale. Fluids will utilize fractures present in low-permeability media to initiate or extend

preferential dissolution channels. In our experiment, dissolution pathways were guided both by variably distributed physical features (microfractures) and reactive phase distributions (dolomite vs. anhydrite) that were aligned with depositional bedding. The creation of significant leakage pathways in the field would instead require fractures oriented perpendicular to bedding, assuming horizontal caprock stratigraphy.

Carbonate content may be a useful qualitative metric for the long-term stability of an evaporite, because injection of chemically perturbed fluids (e.g., "wet" supercritical CO_2, CO_2-saturated brines, or make-up waters) will result in carbonate mineral dissolution and new voidspace creation. Fast-reacting anhydrite may also contribute to porosity changes from injection of dilute water as a make-up fluid, but not as a direct result of CO_2 injection. We have shown that for a highly impermeable rock such as an evaporite, preferential carbonate dissolution leads to the formation of localized channels if the caprock is continually exposed to undersaturated fluids. An indirect effect of preferential carbonate reactivity is voidspace production through physical transport of anhydrite and silicates liberated from the rock matrix by dissolution of a more reactive phase (here, dolomite).

In our experiment, residual anhydrite and silicate minerals were transported out of the experimental system without contributing to the dissolved chemical load. It is possible that such freed mineral phases could accumulate in pore throats downstream of the reaction front in a caprock. Once an EOR field has been transitioned to carbon storage and CO_2/water flooding ceases, permeability changes as a result of chemical and pressure perturbations should decrease. Our experiment shows that dolomite kinetics attain equilibrium over short lengthscales. This process could effectively shut down the generation of new voidspace and the development of established preferential pathways.

ASSOCIATED CONTENT

Supporting Information

Table 1, composition of experimental brine; Figure 1, mercury porosimetry results; Figure 2, wormhole volume occupied per gray-scale zone; Table 2, effluent chemistry. This material is available free of charge via the Internet at http://pubs.acs.org.

Supporting Information Table 1. Composition and fluid saturation indices of experimental brine solution.

Reagent-grade salt	**mole · kg H_2O^{-1}**
NaCl	1.01
$NaHCO_3$	0.00792
Na_2SO_4	0.0369
$CaCl_2{\cdot}2H_2O$	0.0353
$MgCl_2{\cdot}6H_2O$	0.0159
Mineral, conditions	**Saturation Index**
dolomite, 60°C, CO_2-free	2.56
dolomite, 60°C, 3 MPa pCO_2	-2.70
anhydrite, 60°C, CO_2-free	-0.3
anhydrite, 60°C, 3 MPa pCO_2	-0.03

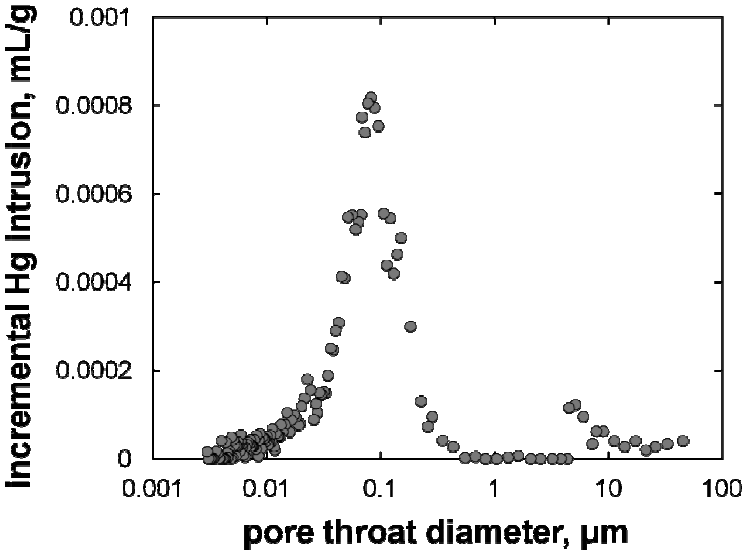

Supporting Information Figure 1. Pore throat diameter distribution from mercury intrusion porosimetry conducted on adjacent Three Fingers core sample.

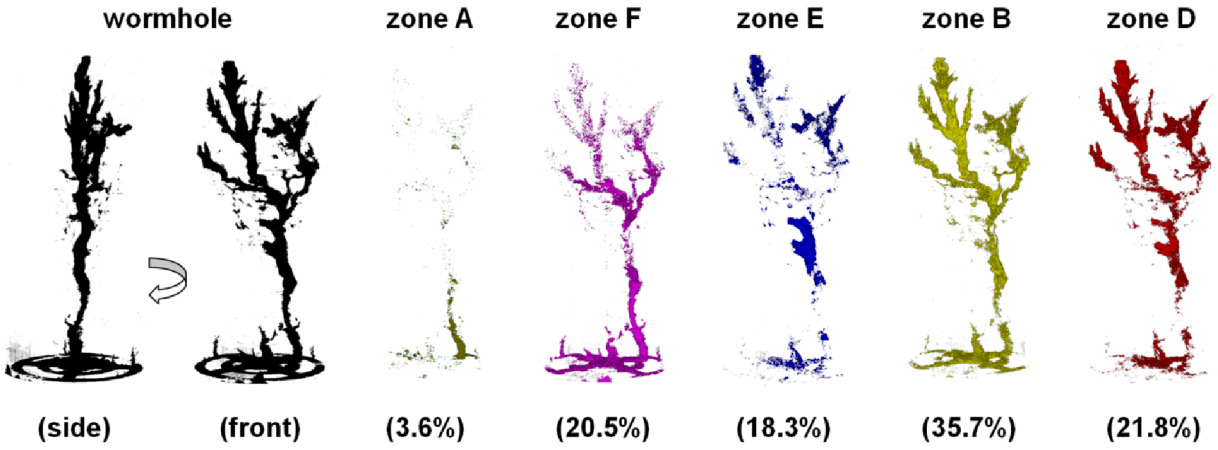

Supporting Information Figure 2. Reconstructed XCMT image of wormhole dissolved volume (side, front) and distributions of individual zones within dissolved wormhole region. See Table 1 for complete zone descriptions.

Supporting Information Table 2. Major component solution chemistry data.

time	Al	Ca	Fe	Mg	Mn	Si	SO4	Sr
[days]	[mol/L]	[mol/L]	[mol/L]	[mol/L]	[mol/L]	[mol/L]	[mol/L]	[mol/L]
-4.36	4.35e-07	4.19e-02	7.39e-05	1.64e-02	1.02e-05	4.76e-05	4.46e-02	2.19e-04
-2.67	2.51e-07	4.09e-02	6.62e-05	1.58e-02	6.87e-06	4.06e-05	4.43e-02	1.71e-04
-1.26	4.14e-07	4.32e-02	6.81e-05	1.67e-02	5.15e-06	3.96e-05	4.36e-02	1.52e-04
0.17	3.60e-07	4.20e-02	7.32e-05	1.58e-02	4.35e-06	4.22e-05	4.63e-02	1.42e-04
0.66	1.30e-06	4.58e-02	1.32e-04	2.00e-02	4.88e-06	1.61e-04	4.12e-02	1.31e-04
1.67	2.35e-06	4.85e-02	1.51e-04	2.32e-02	9.15e-06	1.29e-04	3.93e-02	1.15e-04
2.65	2.80e-06	4.58e-02	1.37e-04	2.24e-02	9.59e-06	1.01e-04	3.88e-02	9.54e-05
5.66	3.56e-06	4.83e-02	1.32e-04	2.43e-02	7.51e-06	5.45e-05	3.68e-02	5.48e-05
6.61	3.70e-06	5.52e-02	1.27e-04	2.42e-02	6.58e-06	5.42e-05	3.76e-02	4.81e-05
8.66	4.52e-06	4.54e-02	1.24e-04	2.57e-02	5.04e-06	3.12e-05	3.74e-02	3.25e-05
10.08	5.13e-06	5.08e-02	1.25e-04	2.60e-02	4.18e-06	1.92e-05	3.70e-02	2.10e-05
11.97	9.69e-07	4.09e-02	7.97e-05	1.82e-02	5.72e-07	1.08e-06	3.59e-02	5.17e-06
12.97	1.31e-06	4.13e-02	7.91e-05	1.80e-02	4.31e-07	1.07e-06	3.69e-02	5.03e-06

time	TIC	pH
[days]	[mol/L]	[pH]
-4.36	4.25e-03	6.89
-2.67	4.10e-03	7.13
-1.26	4.09e-03	7.16
1.08	1.26e-01	5.45
2.13	1.72e-01	5.37
3.09	2.12e-01	5.24
7.15	3.12e-01	5.22

9.14	3.26e-01	5.12
10.21	3.58e-01	5.14

AUTHOR INFORMATION

Corresponding Author

*E-mail address: megan@llnl.gov; Tel.: 925.423.7970.

Present Addresses

Lawrence Livermore National Laboratory, 7000 East Avenue L-231, Livermore, CA 94550, United States

† this information may be included here.

Author Contributions

The manuscript was written through contributions of all authors. All authors have given approval to the final version of the manuscript.

ACKNOWLEDGMENTS

The authors are grateful for the efforts of LLNL personnel Victoria Genetti and Rachel Lindvall for ICP-MS analyses, Harris Mason for image analysis assistance, Rick Kemptner and

Dave Ruddle for experimental fabrication, Sharon Torres for SEM data acquisition, and Harris Mason for image analysis assistance. Alastair MacDowell and Dula Parkinson (ALS, LBNL) and Paul Tafforeau (ESRF) were instrumental in the acquisition of XCMT data. Ian Hutcheons and Maurice Shevalier (Univ. of Calgary) graciously shared their extensive petrologic data.

Funding for this work was provided from both the U.S. Department of Energy and the Petroleum Research Technology Centre (PTRC), IEA GHG Weyburn-Monitoring and Storage Project.

DISCLAIMER

This document was prepared as an account of work sponsored by an agency of the United States government. Neither the United States government nor Lawrence Livermore National Security, LLC, nor any of their employees makes any warranty, expressed or implied, or assumes any legal liability or responsibility for the accuracy, completeness, or usefulness of any information, apparatus, product, or process disclosed, or represents that its use would not infringe privately owned rights. Reference herein to any specific commercial product, process, or service by trade name, trademark, manufacturer, or otherwise does not necessarily constitute or imply its endorsement, recommendation, or favoring by the United States government or Lawrence Livermore National Security, LLC. The views and opinions of authors expressed herein do not necessarily state or reflect those of the United States government or Lawrence Livermore National Security, LLC, and shall not be used for advertising or product endorsement purposes.

AUSPICES STATEMENT

This work performed under the auspices of the U.S. Department of Energy by Lawrence Livermore National Laboratory under Contract DE-AC52-07NA27344. LLNL-XX-XXXX.

ABBREVIATIONS

CO_2, carbon dioxide; EOR, enhanced oil recovery; GCS, geologic carbon storage.

REFERENCES

(1) Carbon Dioxide Capture & Storage Projects Map; http://sequestration.mit.edu/tools/map_Projects.html.

(2) United States Department of Energy. *Carbon Sequestration Atlas III of the United States and Canada – Version 3*; National Energy Technology Laboratory: Morgantown, WV, **2010**; http://www.netl.doe.give/technologies/carbon_seq/refshlf/atlasIII/2010atlasIII.pdf.

(3) Shiraki, R.; Dunn, T.L. Experimental study on water-rock interactions during CO_2 flooding in the Tensleep Formation, Wyoming, USA. *Appl. Geochem*. **2000**, *15*, 265-279; DOI 10.1016/S0883-2927(99)00048-7.

(4) Kaszuba, J.P.; Janecky, D.R.; Snow, M.G. Experimental evaluation of mixed fluid reactions between supercritical carbon dioxide and NaCl brine: Relevance to the integrity of a geologic carbon repository. *Chem. Geol*. **2005**, *217*, 277-293; DOI 10.1016/j.chem.geo.2004.12.014.

(5) Carey, J.W.; Wigand, M.; Chipera, S.J., WoldeGabriel, G.; Pawar, R.; Lichtner, P.; Wehner, S.C.; Raines, M.A.; Guthrie, Jr., G.D. Analysis and performance of oil well cement with 30 years of CO_2 exposure from the SACROC unit, West Texas, USA. *Int. J. Greenhouse Gas Control* **2007**, *1*, 75-85; DOI 10.1016/S1750-5836(06)00004-1.

(6) Andreani, M.; Gouze, P.; Luquot, L.; Jouanna, P. Changes in seal capacity of fractured claystone caprocks induced by dissolved and gaseous CO_2 seepage. *Geophys. Res. Letters* **2008**, *35*, L14404; DOI 10.1029/2008GL034467.

(7) Angeli, M.; Soldal, M.; Skurtveit, E.; Aker, E. Experimental percolation of supercritical CO_2 through a caprock. *Ener. Proc*. **2009**, *1*, 3351-3358; DOI 10.1016/j.egypro.2009.02.123.

(8) Ellis, B.; Peters, C.; Fitts, J.; Bromhal, G.; McIntyre, D.; Warzinski, R. Rosenbaum, E. Deterioration of a fractured carbonate caprock exposed to CO_2-acidified brine flow. *Greenhouse Gas Sci. Technol*. **2011**, *1*, 248-260; DOI 10.1002/ghg.

(9) Shukla, R.; RAnjith, P.; Haque, A.; Choi, X. A review on studies on CO_2 sequestration and caprock integrity. *Fuel* **2010**, *89*, 2651-2664; DOI 10.1016/j.fuel.2010.05.012.

(10) Li, Z; Dong, M.; Li, S.; Huang, S. CO_2 sequestration in depleted oil and gas reservoirs – caprock characterization and storage capacity. *Ener. Conv. & Mgmt*. **2006**, *I*, 1372-1382; DOI 10.1016/j.enconman.2005.08.023.

(11) Hangx, S.J.T.; Spiers, C.J.; Peach, C.J. Mechanical behavior of anhydrite caprock and implication for CO_2 sealing capacity. *J. Geophys. Res*. **2011**, *115*, B0742; DOI 10.1029/2009JB006954.

(12) Weyburn-Midale CO_2 Project; Petroleum Technology Research Centre: www.ptrc.ca/weyburn_overview.php.

(13) Emberley, S.; Hutcheon, I.; Shevalier, M.; Durocher, K.; Mayer, B.; Gunter, W.D.; Perkins, E.H. Monitoring of fluid-rock interaction and CO_2 storage through produced fluid sampling at the Weyburn CO_2-injection enhanced oil recovery site, Saskatchewan, Canada. *Appl. Geochem*. **2005**, *20*, 1131-1157; DOI 10.1016/j.apgeochem.2005.02.007.

(14) Raistrick, M.; Mayer, B.; Shevalier, M.; Perex, R.J.; Hutcheon, I.; Perkins, E.; Gunter, B. Using chemical and isotopic data to quantify ionic trapping of injected carbon dioxide in oil field brines. *Env. Sci. & Technol*. **2006**, *40*, 6744-6749; DOI 10.1021/es060551a.

(15) Smith, M.M.; Sholokhova, Y.; Hao, Y.; Carroll, S.A. Evolution of carbonate dissolution features produced under variable pCO_2 conditions relevant to CO_2-EOR and Geologic CO_2 Storage. In review.

(16) Durocher, K.; Hutcheon, I.; Shevalier, M.; Mayer, B.; Gunter, B.; Perkins, E.; Bloch, J. Reservoir (baseline) mineralogy final report; Subtask 3.1; *IEA Weyburn CO_2 Monitoring and Storage Project*, Petroleum Technology Research Centre, **2003**.

(17) Rasband, W.S. ImageJ. United States National Institutes of Health: Bethesda, MD, **1997-2012**; http://imagej.nih.gov/ij/.

(18) Peters, C. Accessibilities of reactive minerals in consolidated sedimentary rock: An imaging study of three sandstones. *Chem. Geol*. **2009**, *265*, 198-208; DOI 10.1016/j.chemgeo.2008.11.014.

(19) Wolery, T.W. EQ3/6, a software package for geochemical modeling of aqueous systems. UCRL MA-110662-PT-1, Lawrence Livermore National Laboratory: Livermore, CA, **1992**.

(20) Hoefner, M.L.; Fogler, H.S. Pore evolution and channel formation during flow and reaction in porous media. *AiChE Jour*. **1998**, *34*, 45-54; DOI 10.1002/aic.690340107.

(21) Fredd, C.N.; Fogler, H.S. Influence of transport and reaction on wormhole formation in porous media. *AiChE Jour.* **1998**, *44*, 1933-1949; DOI 10.1002/aic.690440902.

(22) Cohen, C.E.; Ding, D.; Quintard, M.; Bazin, B. From pore scale to wellbore scale: Impact of geometry on wormhole growth in carbonate acidization. *Chem. Eng. Sci.* **2008**, *63*, 3088-3099; DOI 10.1016/j.ces.2008.03.021.

(23) Daccord, G.; Lietard, O.; Lenormand, R. Chemical dissolution of a porous medium by a reactive fluid – II. Convection vs reaction, behavior diagram. *Chem. Eng. Sci.* **1993**, *48*, 179-186; DOI 10.1016/0009-2509(93)80294-Z.

(24) Golfier, F.; Zarcone, C.; Bazin, B.; Lenormand, R.; Lasseux, D.; Quintard, M. On the ability of a Darcy-scale model to capture wormhole formation during the dissolution of a porous medium. J. *Fluid. Mech*. **2002**, *457*, 213-254; DOI 10.1017/S0022112002007735.

(25) Newell, D.L.; Viswanathan, H.S.; Lichtner, P.C., Carey, J.W.; Thyne, G.; Kaszuba, J.P. Experimental determination of supercritical CO_2 mass transfer rates into brine, *American Geophysical Union Fall Meeting*, San Francisco, CA, December 6-10, 2011.

(26) Gherardi, F.; Xu, T.; Pruess, K. Numerical modeling of self-limiting and self-enhancing caprock alteration induced by CO_2 storage in a depleted gas reservoir. *Chem. Geol*. **2007**, *244*, 102-129; DOI 10.1016/j.chemgeo.2007.06.009.

(27) Rosenbauer, R.J.; Koksalan, T. Palandri, J.L. Experimental investigation of CO_2-brine-rock interactions at elevated temperature and pressure: Implications for CO_2 sequestration in deep-saline aquifers. *Fuel Process. Technol*. **2005**, *86*, 1581-1597; DOI 10.1016/j.fuproc.2005.01.011.

(28) Plummer, L.N.; Busby, J.F.; Lee, J.W.; Hanshaw, B.B. Geochemical mondeling of the Madison aquifer in parts of Montana, Wyoming, and South Dakota. *Water. Resour. Res*. **1990**, *26*, 1981-2014; DOI 10.1029/WR026i009p01981.

(29) Kuhn, M.; Clauser, C.; Vosbeck, K.; Stanjek, H.; Meyn, V.; Back, M.; Peiffer, S. Mineral trapping of CO_2 in operated hydrogeothermal reservoirs. In *Carbon Dioxide Sequestration in Geological Media – State of the Science*; Grobe, M.; Pashin, J.C.; Dodge, R.I., Eds. AAPG Studies in Geology, **2009**, *59*, pp8.

TABLE OF CONTENTS ARTWORK